Performance Evaluation of Wind Decontamination System by Computational Fluid Dynamics

Li, Cong
Faculty of Marine and Civil Engineering, Dalian Ocean University | Interdisciplinary Graduate School of Engineering Sciences, Kyushu University

Ito, Kazuhide
Interdisciplinary Graduate School of Engineering Sciences, Kyushu University

https://doi.org/10.5109/1495158

出版情報：Evergreen. 1 (2), pp.12-17, 2014-09. Green Asia Education Center
バージョン：

Performance Evaluation of Wind Decontamination System by Computational Fluid Dynamics

Cong Li[1,2] , Kazuhide Ito[2*]

[1] Faculty of Marine and Civil Engineering, Dalian Ocean University, China

[2] Interdisciplinary Graduate School of Engineering Sciences, Kyushu University, Japan

*Author to whom correspondence should be addressed, E-mail: ito@kyudai.jp

(Received July 31, 2014; accepted August 31, 2014)

In the event of a severe nuclear, biological, or chemical (NBC) incident, perhaps related to terrorism or a nuclear power plant accident, rapid and effective decontamination procedures for the human body become critically important during on-site rescue operations. In this study, we propose a new decontamination system based on forced convection, called the wind decontamination system (WDCS). The fundamental performance of a WDCS prototype is evaluated by using computational fluid dynamics (CFD). The mass transfer characteristics of the WDCS air jets that act on the human body are quantitatively discussed, based on the CFD results.

Keywords: Computational Fluid Dynamics, Wind Decontamination System, Mass Transfer coefficient

1. Introduction

The necessity of developing a prompt and effective decontamination system for the outer surface of the human body has been brought into prominence by the severe incident at Fukushima Daiichi nuclear power plant in 2011. From the perspective of on-site rescue at the scene of a disaster, wet and dry decontamination processes are both regarded as universally applicable and basic countermeasures (Okumura T., 1998a and 1998b, Bronstein and Currance, 1994), especially in a chemical accident scenario involving gaseous or liquid contaminants. However, both wet and dry decontamination processes have limitations. A water-based decontamination procedure has an advantage in decontamination efficiency, but it is difficult to provide privacy to victims during the decontamination process because of the necessity of undressing. Furthermore, it is also difficult to set up the decontamination device quickly because of the limitations of hot-water preparation and on-site requirements of the water-pool. In a severe disaster scenario where hundreds of victims are exposed to hazardous contaminants, an effective and rapid decontamination method is required that can respond rapidly while also reducing the feeling of panic among the victims.

The primary objective of this study is to develop a novel decontamination procedure that uses forced convective flow, called the wind decontamination system (WDCS). The operating principle of the WDCS is similar to that of an industrial air-shower system. Although industrial air-shower systems have been widely adopted in factories and cleanrooms, a quantitative and qualitative method to evaluate their decontamination efficiency has not yet been fully discussed (Austin, 1970, Li and Ito, 2012, Li and Ito, 2014). In general, such a system has a conservative design, in consideration of the safety rate. From this background, the purpose of this

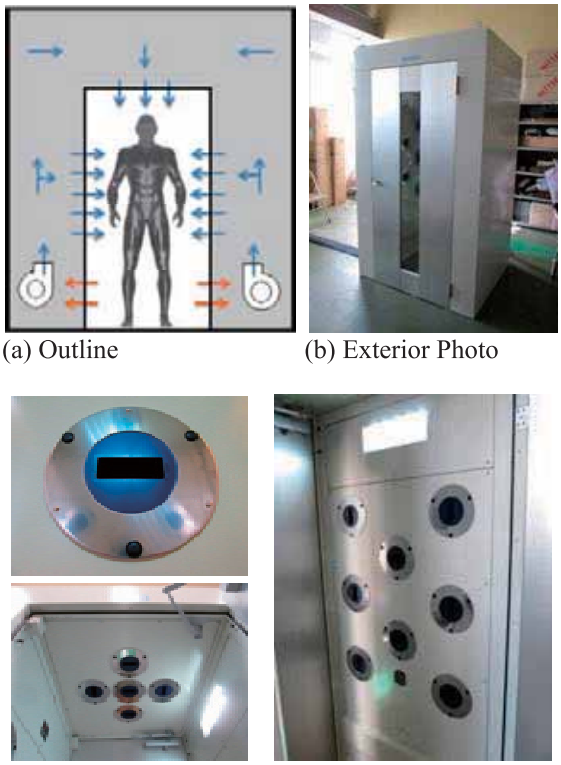

(a) Outline (b) Exterior Photo

(c) Supply nozzles (d) Supply nozzles on the wall

Fig. 1. Exterior and interior spaces of the WDCS prototype.

study is to discuss an optimized design method for a WDCS and an index of decontamination efficiency for a WDCS.

In previous research, we have evaluated the decontamination performance of an industrial air-shower system by experiment and computational fluid dynamics (CFD), and discussed the design of a WDCS prototype (Li and Ito, 2014). Following from this research, the purpose of this study is to conduct CFD simulations in accordance with experimental scenarios that target the detailed geometry of a WDCS, and to provide additional fundamental information applicable to the design of a WDCS. In particular, the mass transfer from the human body surface caused by a WDCS prototype is discussed as a fundamental index for the evaluation of the decontamination efficiency, based on the CFD results.

2. WDCS prototype

Figure 1 shows the outline of the WDCS prototype. The entry and exit doors are designed for rapid, one-way handling for in-order treatment of large numbers of casualties. There are a total of 21 supply nozzles placed on the side walls and ceiling. Each nozzle (detailed in Figure 1(c)) has a rectangular opening of area 1700 mm^2, and can oscillate along the shorter axis at 2.0 Hz, causing periodic fluctuation of flow jet direction. The 5 nozzles that are fixed on the ceiling are used to generate a uniform vertical flow from the top to bottom, in order to prevent recirculation of the contaminant. A total of 16 nozzles are installed on the side walls (Figure 1(d)), to ensure the purging of the contaminant from the local dead zones of the human body. The maximum airflow rate was 25 m^3/min (1500 m^3/h). Under this condition, the average inlet supply velocity of each nozzle is 12 m/s.

We have previously reported the results regarding the performance evaluation of an industrial air-shower system in removal of gaseous and liquid contaminants from the human body surface. With the objective of a portable decontamination operation, the WDCS prototype in this study is smaller and lighter than the industrial air-shower system previously investigated (Li and Ito, 2014). The airflow rate is also approximately reduced by half, with each nozzle having an equal flow. In addition, the self-induced oscillating jet from the flip-flop nozzle was adopted in the WDCS prototype, in order to increase the decontamination performance. The experimental results for fundamental decontamination efficiency have been reported in previous papers (Li et al., 2013, Li and Ito, 2014).

3 Outline of CFD simulation

3.1 Numerical and boundary conditions

In this study, a CFD simulation was conducted to investigate the performance of a WDCS prototype. Figure 2 shows the outline of target space for numerical

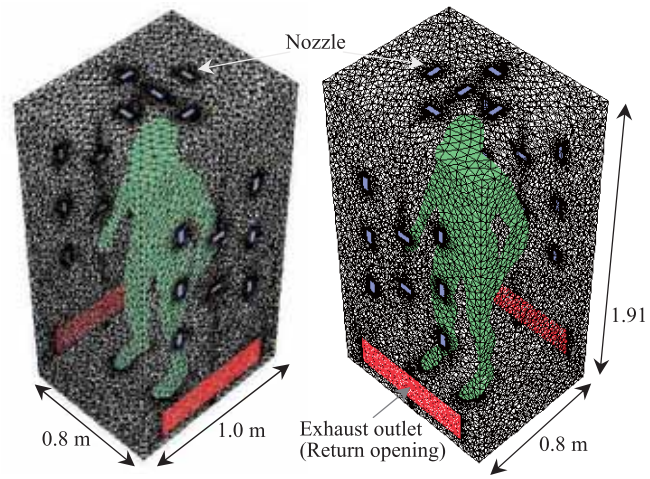

(a) Cross wind condition (b) Facing wind condition

Fig. 2. Numerical Analysis Domains

Table 1. Numerical and boundary conditions.

Turbulence Model	SST k-ω model (3-D. calc.)
Algorithm	SIMPLE (Steady and Unsteady)
Scheme	Convection : QUICK
Inflow boundary	Area of inlet : 1700 mm^2 Total air flow rate: 25 m^3/min Velocity magnitude : 12 m/s
Inflow direction	Steady: Perpendicular to wall Oscillating: 2.0 Hz vibration Turbulent Intensity: 10, 30 and 50%
Outflow boundary	$U_{out} = k_{out} = \varepsilon_{out}$ = Free slip
Wall treatment (incl. human model)	Velocity : No slip, k_{wall} : No slip Scalar (temp.): gradient zero ($\partial T/\partial x = 0$)

Table 2. Cases analyzed.

Cases	Wind direction (relative position)	Air supply direction	*TI* [%]
Case C-S	Cross wind	(A) Steady	10
Case C-O2		(C) Oscillating	10
Case C-O3			30
Case C-O4			50
Case F-S	Facing wind	(A) Steady	10
Case F-O2		(C) Oscillating	10
Case F-O3			30
Case F-O4			50

simulation with a virtual manikin arranged in the center of the room (Ito and Hotta, 2006, Li and Ito, 2013). The triangular surface mesh reproduced the complex geometry of the human body shape. Prism cells were used to solve the boundary layer around the body. A minimum of four continuous layers of prism cells were allocated, with equal heights of less than 1.0 mm. The wall units (y^+) that express the dimensionless normal distance from the surface approximately met the requirement of 1.0 over the whole surface of the body.

Two different wind conditions are considered: (1) The body facing the door (cross wind), with (x, y, z) dimensions of (0.8 m, 1.91 m, 1.0 m), and (2) the body facing the wall (facing wind), with dimensions of (1.0 m,

1.91 m, 0.8 m). The virtual manikin is representative of realistic human body proportions for an adult male.

The numerical and boundary conditions are listed in Table 1. The total airflow rate follows the performance of the WDCS prototype and is set to 25 m^3/min (1500 m^3/h). Correspondingly, the velocity magnitude of each supply inlet (nozzle) in the CFD simulation is 12 m/s. In view of the strong wind conditions, i.e., in excess of 10 m/s, the SST k-ω model was employed in CFD simulation (Menter et al., 2003). The SIMPLE algorithm was used with the QUICK scheme for the convective terms, and a second-order central difference scheme was used for the others. In addition, the turbulence intensity is set to either 10%, 30% and 50%. The inlet air temperature T_{air} and the skin surface temperature T_{sk} are set at the fixed values of T_{air} = 293 K and T_{sk} = 307 K. Detailed information is listed in Table 1. In this CFD simulation, the body was assumed to be unclothed.

3.2 Cases analyzed by CFD simulation

The cases analyzed by CFD simulation are listed in Table 2. Here, both steady-state (nozzles perpendicular to the wall, hereafter referred to as steady) and unsteady-state (oscillation at 2.0 Hz, hereafter referred to as oscillating) simulations are carried out. Under the oscillating conditions, a time period of 10 s was simulated. Furthermore, in order to investigate the removal efficiency of the contaminant from the human body, we analyze the distribution of the convective heat transfer coefficient α_c around the body. The mass transfer coefficient can be estimated by assuming the Lewis analogy between heat transfer and mass transfer, and hence the analysis results for the convective heat transfer coefficient can provide fundamental information about the contaminant removal performance, as a first approximation to the parameters that influence a WDCS design.

The convective heat transfer coefficient α_c [W/m^2/K] can be obtained from the following equation (Eq.1):

$$\alpha_c = \frac{Q_c}{T_{sk} - T_{air}} \qquad (1)$$

Here, Q_c [W/m^2] denotes the convective heat flux. T_{sk} and T_{air} represent the skin surface temperature and inlet air temperature respectively. Because the entire wall boundaries were set as fixed temperatures, the analysis for radiative heat transfer was disregarded in this CFD simulation.

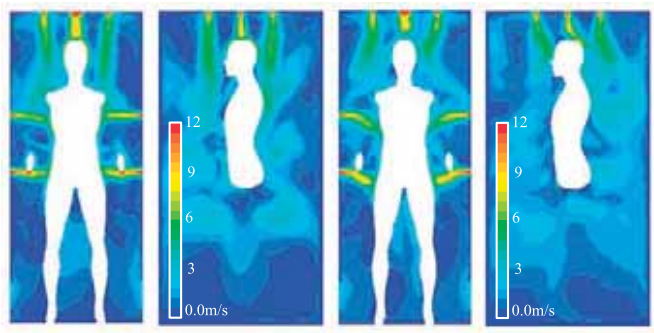

(a) Case C-S (Steady) (b) Case C-O2 (Oscillating)

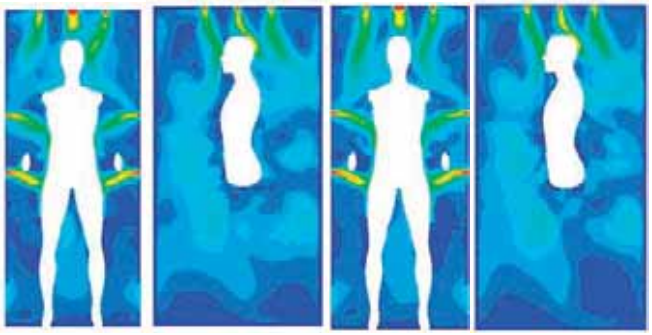

(c) Case C-O3 (Oscillating) (d) Case C-O4 (Oscillating)

Fig. 3. Flow field distributions with a cross wind (velocity magnitude).

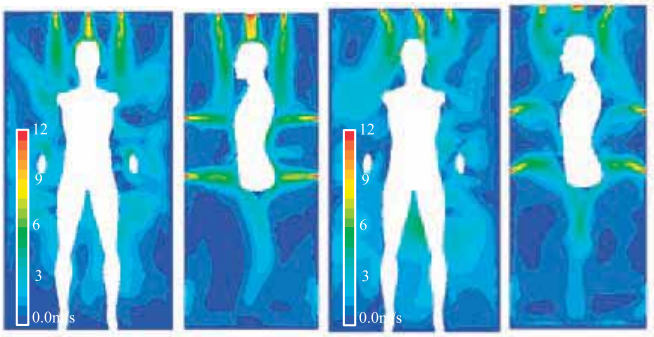

(a) Case F-S (Steady) (b) Case F-O2 (Oscillating)

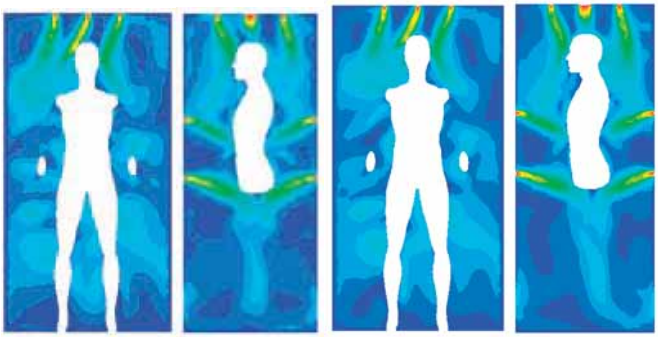

(c) Case F-O3 (Oscillating) (d) Case F-O4 (Oscillating)

Fig. 4. Flow field distributions with a facing wind (velocity magnitude).

4 Results of CFD simulations

4.1 Distribution of flow field

The flow field distribution around the body for the cross wind cases are shown by x-z (left) and y-z (right) view sections in Figure 3. From the y-z view sections, it can be seen that the region of low velocity is wider under the oscillating condition than it is under the steady condition. In the steady condition, the air flow from the ceiling nozzles impinges directly against the head of the human body, and the air flow from the wall nozzles parts from the rear and back of the body. The measured velocity above the head was about 6 m/s. In the

oscillating condition (fluctuating airflow at 2.0 Hz), the velocity around the head in the unsteady air flow was also 6 m/s. For the nozzles on the side walls, the range of velocities around the body segments from the chest to the abdomen was smaller under the oscillating condition than it under the steady condition as shown in Figures 3(a) and (b). The range of velocities around the feet was larger in the oscillating condition than it was in the steady condition.

A lower velocity range around the human body was obtained in the oscillating condition compared to the steady condition. A relatively uniform and well-mixed flow field was observed under the oscillating condition.

Figure 4 shows the flow field distribution for the facing wind cases. Similar to the cross wind, the low velocity region was more widely distributed under the oscillating condition than under the steady condition. Additionally, the contributions of the nozzles on the ceiling and the walls to the head, chest, back, and the feet, were similar to those in cross wind.

4.2 Convective heat transfer coefficient

The distributions of the convective heat transfer coefficient α_c under cross wind are shown in Figure 5. For the oscillating conditions, time averages of values over a period of 10 s are shown in the figures. The distributions of α_c are very similar in the steady and oscillating conditions. Relatively large values of α_c appear at the top of the head, side of the body, and upper part of the thighs. The differences of α_c between body parts are found to be larger in the steady condition than in the oscillating condition.

Figure 6 shows distributions of α_c under the facing wind. Similar to the result under cross wind, the distributions of α_c are nearly the same in the steady condition and the oscillating condition. Relatively large values of α_c are found on the front of the abdomen, back, back of pelvis, and thighs.

The average values of the convective heat transfer coefficient α_c [W/m^2/K] and its standard deviations σ are listed in Tables 3 and 4, for each body segment. The α_c values were relatively large in the steady condition compared to those in the oscillating condition, for almost all body segments. The relatively high velocity jets from nozzles were impinged against the human body in case of the steady condition and the convective heat transfer coefficients α_c were greatly evaluated in the parts. However, the standard deviations σ were smaller in the oscillating condition. The periodically oscillating jets from the supply nozzles caused a relatively homogeneous distribution of α_c on the surface of the body.

The two different wind directions interacting with the human body were set up and analyzed by CFD simulations, and significant differences exist in the results obtained under each of these two wind directions. Especially, significant differences of flow pattern around human body and also the α_c distributions on the human

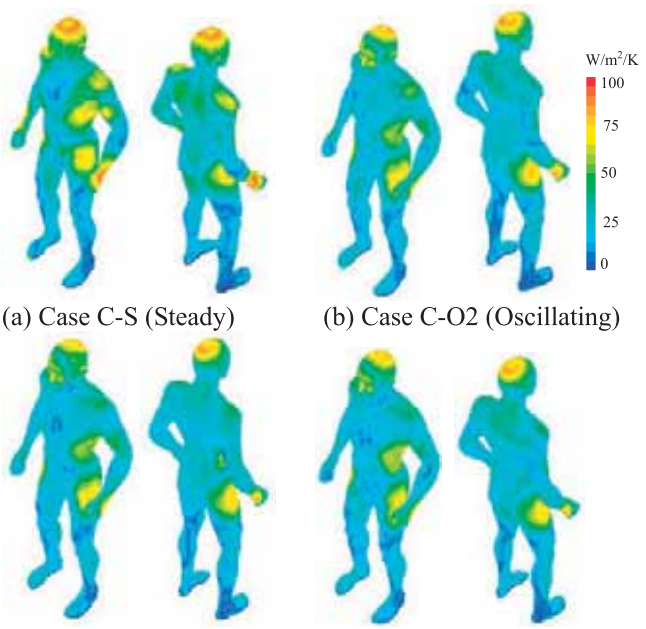

(a) Case C-S (Steady) (b) Case C-O2 (Oscillating)

(c) Case C-O3 (Oscillating) (d) Case C-O4 (Oscillating)

Fig. 5. Convective heat transfer coefficient α_c distributions with a cross wind.

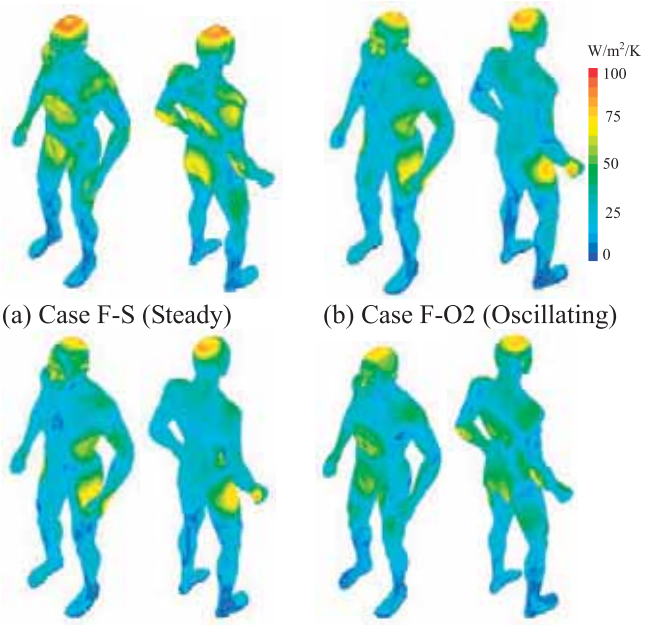

(a) Case F-S (Steady) (b) Case F-O2 (Oscillating)

(c) Case F-O3 (Oscillating) (d) Case F-O4 (Oscillating)

Fig. 6. Convective heat transfer coefficient α_c distributions with a facing wind.

body surfaces were observed in the two different wind directions. However, it is seen that the impact of the wind direction on the area-averaged convective heat transfer coefficient α_c for whole body is small in both two cases (steady and oscillating conditions) as shown in Tables 3 and 4.

In a comparison of the different oscillating conditions, the change of the turbulent intensity *TI* of the air supplied by the nozzles (*TI* = 10%, 30%, and 50%) had no definite impact on the estimated results of average α_c.

In the vicinity of supply nozzle, the velocity gradient of supplied jet and surrounding air was huge and turbulent kinetic energy was generated in proportion to the large velocity gradients. This is one of the causes of no-observed impact of *TI* setting as supply inlet boundary condition of the nozzles.

5. Conclusions

The concept of a wind decontamination system (WDCS) is a novel decontamination method that is expected to substitute for dry and wet decontamination procedures.

In this study, we provided additional information about the flow pattern inside the WDCS, and the convective heat transfer characteristics on the human body surface were calculated by CFD simulation.

From the results of flow field and convective heat transfer coefficient, it was confirmed that the oscillation of the inlet air supply jet direction may contribute to an increase in the air-mixing in a WDCS, and increase the uniformity of convective heat transfer coefficients on the human body surfaces. By conducting the CFD simulation with two wind conditions (steady and oscillating conditions), it was found that the differences of the convective heat transfer coefficients between body segments are smaller in the oscillating condition than they are in the steady condition.

There is little previous research that quantitatively clarified the convective heat (and/or mass) transfer phenomena on the human body surface that occur either in an industrial air-shower system or in a WDCS. The CFD results regarding the distributions of the convective heat transfer coefficient α_c on the body surface are useful and valuable for optimizing the design of a WDCS.

Acknowledgements

The authors would like to express their sincere gratitude to Dr. Lim Eunsu and Mr. Takahiro Yamashita for their kind support and beneficial discussions on this research project.

Table 3. Average α_c [W/m^2/K] on each body segment (Cross wind condition).

Segment	(A) Steady		(B) Oscillating *TI*=10%	
	α_c	σ (STD)	α_c	σ (STD)
Neck	39.875	17.477	34.771	17.375
Face	44.010	17.533	33.169	15.362
Back	32.128	9.857	25.127	8.368
Chest	42.248	18.779	33.492	16.433
Pelvis	36.120	17.535	31.606	15.765
Left Shoulder	35.370	15.176	29.783	12.309
Right Shoulder	34.018	16.147	27.837	11.340
Left Arm	32.172	21.698	30.116	12.404
Right Arm	30.793	21.238	31.022	14.890
Left Hand	38.366	21.205	27.994	14.931
Right Hand	39.683	20.540	30.666	17.047
Left Thigh	22.795	10.323	21.681	9.998
Right Thigh	21.999	9.908	21.486	9.790
Left Leg	15.592	6.028	15.781	7.167
Right Leg	15.657	6.061	16.362	6.630
Left Foot	12.409	6.394	15.156	8.584
Right Foot	11.773	6.608	15.408	8.383
Whole body	30.105	18.778	26.374	15.557

Table 4. Average α_c [W/m^2/K] on each body segment (Facing wind condition).

Segment	(A) Steady		(B) Oscillating *TI*=10%	
	α_c	σ (STD)	α_c	σ (STD)
Neck	37.436	16.551	31.696	15.378
Face	41.865	18.183	36.684	16.295
Back	38.980	15.135	31.844	12.248
Chest	36.156	14.415	30.280	13.277
Pelvis	36.452	17.640	31.911	14.674
Left Shoulder	31.995	14.141	27.285	11.267
Right Shoulder	36.371	15.610	28.388	11.584
Left Arm	43.569	17.675	35.631	14.988
Right Arm	42.952	16.567	32.517	13.731
Left Hand	35.607	15.535	27.704	11.923
Right Hand	31.531	15.061	29.754	13.282
Left Thigh	31.136	13.416	28.421	9.601
Right Thigh	29.926	12.183	28.212	10.921
Left Leg	15.632	7.229	13.233	5.159
Right Leg	15.543	6.967	13.734	5.536
Left Foot	15.357	7.546	14.764	6.682
Right Foot	13.568	7.451	14.710	7.537
Whole body	32.036	17.326	27.525	14.952

References

1) ANSYS Fluent 12.1 Theory Guide, (2009).

2) P. R. Austin, *Design and Operation of Clean Rooms*, Business News Pub. Co. (1970).

3) A. C. Bronstein, P. L. Currance, *Emergency Care for Hazardous Materials Exposure*, Second ed., St. Louis, MO: Mosby Lifeline (1994).

4) K. Ito, T. Hotta, "Development of virtual manikins and its grid library for CFD analysis", *Transactions of SHASE (The Society of Heating, Air-Conditioning and Sanitary Engineers of Japan),* **113**, 27-34 (2006) .(In Japanese)

5) C. Li, K. Ito, "Performance evaluation of industrial air-shower system in removal of gas- and liquid-phase

contaminants from human body", *Evergreen—Joint Journal of Novel Carbon Resource Sciences & Green Asia Strategy*, **1**(1), 40-47 (2014).

6) C. Li, K. Ito, "Numerical and experimental estimation of convective heat transfer coefficient of human body under strong forced convective flow", *Journal of Wind Engineering & Industrial Aerodynamics*, **126**, 107-117 (2014).

7) C. Li, K. Ito, "Numerical analysis of convective heat and mass transfer around human body under strong wind", *International Journal of High-Rise Buildings,* **1**(2), 107-116 (2012).

8) Y. Li, S. Someya, T. Koso, S. Aramaki, K. Okamoto, "Characterization of periodic flow structure in a small-scale feedback fluidic oscillator under low-Reynolds-number water flow", *Flow Measurement and Instrumentation*., **33**, 179-187 (2013).

9) F. R. Menter, M. Kuntz, R. Langtry, "Ten years of Industrial experience with the SST turbulence model", in *Turbulence, Heat and Mass Transfer* 4, eds by K. Hanjalic, Y. Nagano, M. Tummers, 625-632 (2003).

10) T. Okumura, K. Suzuki, A. Fukuda, A. Kohama, N. Takasu, S. Ishimatsu, S. Hinohara, "The Tokyo subway sarin attack: disaster management, part 2: hospital response", *Acad. Emerg. Med*., **5**, 618-624 (1998).

11) T. Okumura, K. Suzuki, A. Fukuda, A. Kohama, N. Takasu, S. Ishimatsu, S. Hinohara, "The Tokyo subway sarin attack: disaster management, part 3: national and international response", *Acad. Emerg. Med.,* **5**, 625-628 (1998).